

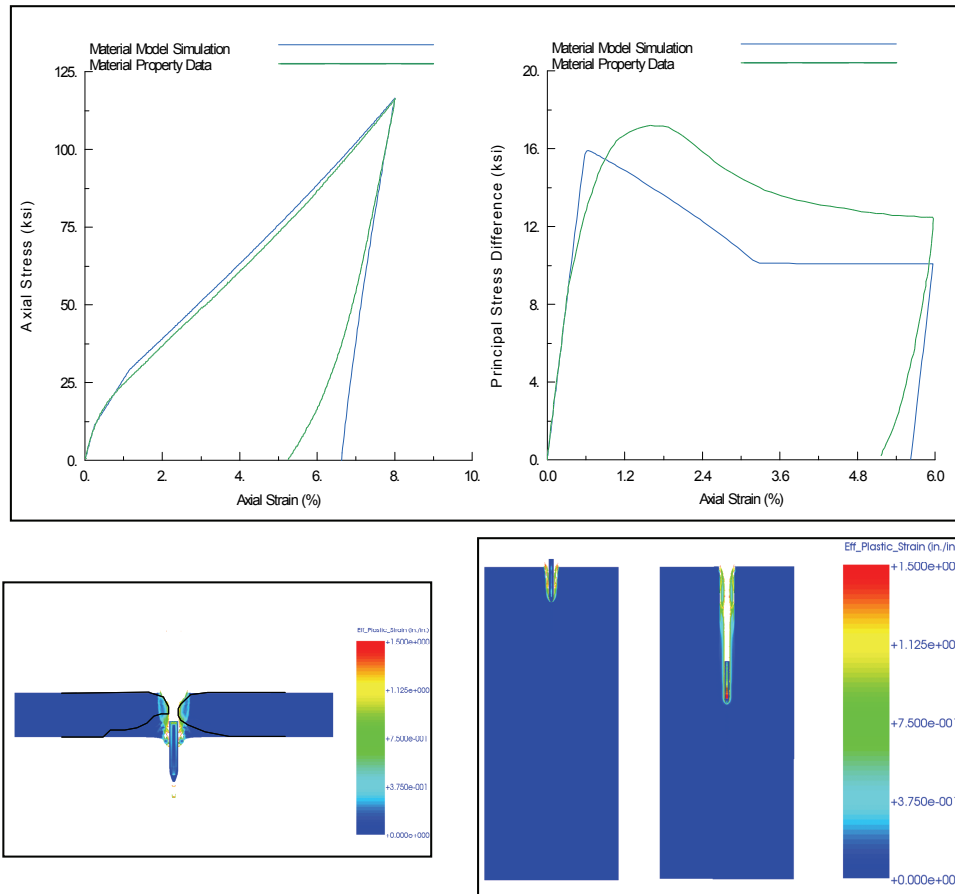


**US Army Corps  
of Engineers®**  
Engineer Research and  
Development Center

## The Advanced Fundamental Concrete (AFC) Model

Mark D. Adley, Andreas O. Frank, Kent T. Danielson,  
Stephen A. Akers, and James L. O'Daniel

November 2010





# The Advanced Fundamental Concrete (AFC) Model

Mark D. Adley, Andreas O. Frank, Kent T. Danielson,  
Stephen A. Akers, and James L. O'Daniel

*Geotechnical and Structures Laboratory  
U.S. Army Engineer Research and Development Center  
3909 Halls Ferry Road  
Vicksburg, MS 39180-6199*

Final report

Approved for public release; distribution is unlimited.

Prepared for Headquarters, U.S. Army Corps of Engineers  
Washington, DC 20314-1000

Under Army Technology Objective D.FP.2009.05  
Defeat of Emerging Adaptive Threats (DEFEAT)

and Hardened Combined Effects Penetrator Warheads (HCEPW) Work Package

**Abstract:** A new constitutive model, the Advanced Fundamental Concrete (AFC) model, was developed for simulating the penetration of projectiles into concrete. Although relatively simple, the model is very robust and fast-running and contains a three-invariant failure surface and nonlinear loading and unloading in hydrostatic compression. This new capability is an adjunct to the Virtual Penetration Laboratory (VPL) software package to address the challenges of determining penetration resistance (PR) equations for high-strength concretes. The Continuous Evolutionary Algorithms automatic fitting routine was used to fit the new model to laboratory mechanical properties for two high-strength concretes. These model fits were implemented into a finite-element code and used in numerical simulations of projectile perforation and penetration experiments. Initial comparisons between results of the simulations and the experiments indicate that the AFC model shows significant promise for use in numerical simulations involving concrete and high-strength geologic materials. Finally, the AFC model in conjunction with the VPL software package was used to develop a PR equation for a high-strength concrete.

**DISCLAIMER:** The contents of this report are not to be used for advertising, publication, or promotional purposes. Citation of trade names does not constitute an official endorsement or approval of the use of such commercial products. All product names and trademarks cited are the property of their respective owners. The findings of this report are not to be construed as an official Department of the Army position unless so designated by other authorized documents.

**DESTROY THIS REPORT WHEN NO LONGER NEEDED. DO NOT RETURN IT TO THE ORIGINATOR.**

# Contents

<b>Figures .....</b>	<b>iv</b>
<b>Preface .....</b>	<b>v</b>
<b>Unit Conversion Factors.....</b>	<b>vi</b>
<b>1   Introduction.....</b>	<b>1</b>
<b>2   Constitutive Model Development.....</b>	<b>3</b>
Model description.....	3
Model fitting algorithm.....	7
Model fits.....	9
Model implementation and testing .....	13
<b>3   Projectile Perforation Simulations.....</b>	<b>14</b>
Perforation experiments .....	14
2D perforation simulations.....	14
<b>4   Projectile Penetration Simulations.....</b>	<b>18</b>
Penetration experiments.....	18
2D penetration simulations .....	18
<b>5   Penetration Resistance Equation for CSPC .....</b>	<b>21</b>
<b>6   Conclusions.....</b>	<b>25</b>
<b>References.....</b>	<b>27</b>
<b>Report Documentation Page</b>	

# Figures

## Figures

Figure 1. The AFC pressure-volume model.....	4
Figure 2. AFC failure surface fit to WES5000 concrete data.....	6
Figure 3. AFC model fit to WES5000 uniaxial strain test data.....	10
Figure 4. AFC model fit to WES5000 triaxial compression data. ....	10
Figure 5. AFC failure surface fit to CSPC concrete data. ....	11
Figure 6. AFC model fit to CSPC uniaxial strain test data.....	12
Figure 7. AFC model fit to CSPC triaxial compression data. ....	12
Figure 8. Representative results from prior perforation experiments; impact ( $V_i$ ) and exit ( $V_e$ ) velocities and final crater shapes are shown. ....	15
Figure 9. EPIC penetration simulation using the AFC model: 127-mm-thick concrete target (time = 10 msec).....	16
Figure 10. EPIC penetration simulation using the AFC model: 216-mm-thick concrete target (time = 10 msec).....	16
Figure 11. EPIC penetration simulation using the AFC model: 254-mm-thick concrete target (time = 15 msec).....	17
Figure 12. EPIC penetration simulations using the AFC model for impact velocities of (a) 300 m/s and (b) 800 m/s. ....	19
Figure 13. EPIC penetration simulation results using the AFC model versus experimental data from ballistic experiments (Cargile et al. 1999). ....	20
Figure 14. Spherical CSPC PR equation developed in the VPL code. ....	23
Figure 15. Cylindrical CSPC PR equation developed in the VPL code.....	23
Figure 16. Comparison of EPIC and VPL predictions with experimental data.....	24

## Preface

The research documented herein was conducted by personnel of the Impact and Explosion Effects Branch (IEEB), Engineering Systems and Materials Division (ESMD), and the Structural Mechanics Branch (SMB), Geosciences and Structures Division (GSD), within the Geotechnical and Structures Laboratory (GSL), U.S. Army Engineer Research and Development Center (ERDC). The research was funded by Headquarters, U.S. Army Corps of Engineers, under Army Technology Objective D.FP.2009.05, Defeat of Emerging Adaptive Threats (DEFEAT), and under the Hardened Combined Effects Penetrator Warheads (HCEPW) Work Package, “HPC Prediction of Weapon Penetration, Blast, and Secondary Effects” work unit. M. Jason Roth was the Work Package Manager for the DEFEAT program, and Dr. J. Donald Cargile was the Work Package Manager for the HCEPW program.

Drs. Mark D. Adley and Andreas O. Frank, IEEB, developed the software and integrated the various algorithms that comprise the Advanced Fundamental Concrete (AFC) model. Dr. Frank also provided the input files for the EPIC code. Dr. Stephen A. Akers, IEEB, provided guidance in selecting the forms of the equations for the model. Drs. Kent T. Danielson, IEEB, and James L. O’Daniel, SMB, provided advice on selection of the algorithms needed for the AFC model. Tracey A. Waddell, IEEB, assisted in preparation of this report.

During this model development effort, Henry S. McDevitt, Jr., was Chief, IEEB; Dr. Gordon W. McMahon was Chief, SMB; Dr. Larry N. Lynch was Chief, ESMD; Bartley P. Durst was Chief, GSD; Dr. William P. Grogan was Deputy Director, GSL; and Dr. David W. Pittman was Director, GSL.

COL Gary E. Johnston was Commander and Executive Director of ERDC. Dr. Jeffery P. Holland was Director.

## Unit Conversion Factors

Multiply	By	To Obtain
feet	0.3048	meters
inches	0.0254	meters
kips (force)	4.448222	kilonewtons
pounds (force) per square inch	6.894757	kilopascals

# 1 Introduction

The Geotechnical and Structures Laboratory at the U.S. Army Engineer Research and Development Center (ERDC) has conducted a significant amount of projectile penetration research. These efforts included numerous projectile penetration experiments using the ERDC 83-mm Projectile Penetration Research Facility (Frew et al. 1993), extensive material property experiments that characterized target mechanical behavior and provided data for fitting constitutive models (Akers et al. 1995), and numerous fully-first-principle calculations of various penetration events (Adley et al. 1996). Our research is focused on gathering data and gaining insight into the processes of penetration mechanics. One of the primary goals of our research is to develop more accurate and robust material models that can be more easily used by an analyst. As the complexity of constitutive models increases, the difficulty of fitting the laboratory material property data to these models also increases. Therefore, a second focus of our efforts is to develop methodologies to reduce the time and effort required to fit the material property data to the models.

As mentioned previously, projectile penetration events can be simulated by using fully “first-principle” methods such as “hydrocodes.” This is accomplished by discretizing both the projectile and the target into a finite number of pieces and allowing the first-principle physics, i.e., conservation of mass, momentum, and energy, to dictate the calculated penetration event. However, these computational methods are extremely resource intensive. Therefore, a third focus of our research efforts is the development of numerical methods for simulating projectile penetration that replace the finite element model of the target with penetration resistance equations that represent the resistance of a target material to penetration.

In this report, we discuss the development of a new constitutive model for simulating concrete penetration by projectiles, i.e., the Advanced Fundamental Concrete (AFC) model. We implemented the new model in the EPIC Lagrangian hydrocode (Johnson et al. 2001), because the source code is readily available to us, and we have used this code for a number of years. It was our intention to develop a relatively simple yet robust model that includes a three-invariant failure surface, because such a model is not currently available in the production version of EPIC. For example,

two-invariant models such as the HJC (Holmquist et al. 1993) and Hull (Johnson et al. 2001) concrete models have their failure surface completely described by only the first two invariants of the stress tensor. It has been shown that the failure surface for many geomaterials (including concrete) may be dependent on all three stress invariants (Fossum and Brannon 2006). For example, the strength observed during compression at a given level of pressure is typically greater than the absolute value of the extension strength at the same pressure.

We also discuss in this report the numerical algorithms used to automatically fit the AFC model to various laboratory material property data. We demonstrate the effectiveness of this new automatic fitting algorithm by developing AFC model fits for two different concrete materials.

Finally, we present validation examples that use the AFC model and the material fits generated to simulate projectile penetration experiments. We also use the validated model and the associated fits in the Virtual Penetration Laboratory (VPL) software package (Adley et al. 2007) to generate a penetration resistance (PR) equation that is used to simulate the aforementioned penetration experiments.

## 2 Constitutive Model Development

### Model description

The AFC model is a three-invariant plasticity model. The model simulates irreversible hydrostatic crushing, material yielding, plastic flow, and damage. The model has a nonlinear, pressure-volume relationship and a linear shear relationship, i.e., constant shear modulus, G. The model also includes strain-rate effects for the failure surface, i.e., increasing shear strength with increasing strain rates. As with most of the simple constitutive models for concrete, our model separates the hydrostatic response from the deviatoric response. Thus, the hydrostatic and deviatoric responses are independently calculated without providing any coupling between the two, i.e., no volumetric strain due to pure deviatoric loading can develop.

First, we will describe the hydrostatic behavior of our model, which includes a nonlinear bulk modulus and irreversible volumetric crushing that contributes to material damage. More specifically, the compressive hydrostatic behavior can be separated into three distinct regions described by an initial elastic zone, followed by an irreversible crushing response, and finally an elastic locking region. Furthermore, the model treats initial loading, unloading, and reloading differently. An overview of the hydrostatic behavior is shown graphically in Figure 1.

The initial elastic zone for the model only occurs for volume strains below the crushing volume strain value ( $U_{crush}$ ). Initial loading, unloading, and reloading in the elastic zone all follow linear-elastic behavior defined by the elastic bulk modulus  $K_e = P_{crush}/U_{crush}$ , where  $P_{crush}$  is the maximum attainable pressure for the initial elastic zone.

The irreversible crushing response occurs for all materials in which the volume strain exceeds the crushing volume strain value ( $U_{crush}$ ) but has not exceeded the locking volume strain value ( $U_{lock}$ ). The crushing region is defined by letting the origin of the crushing response coincide with the point in pressure-volume space with the ending of the initial elastic zone ( $(P_{crush}, U_{crush})$ ).

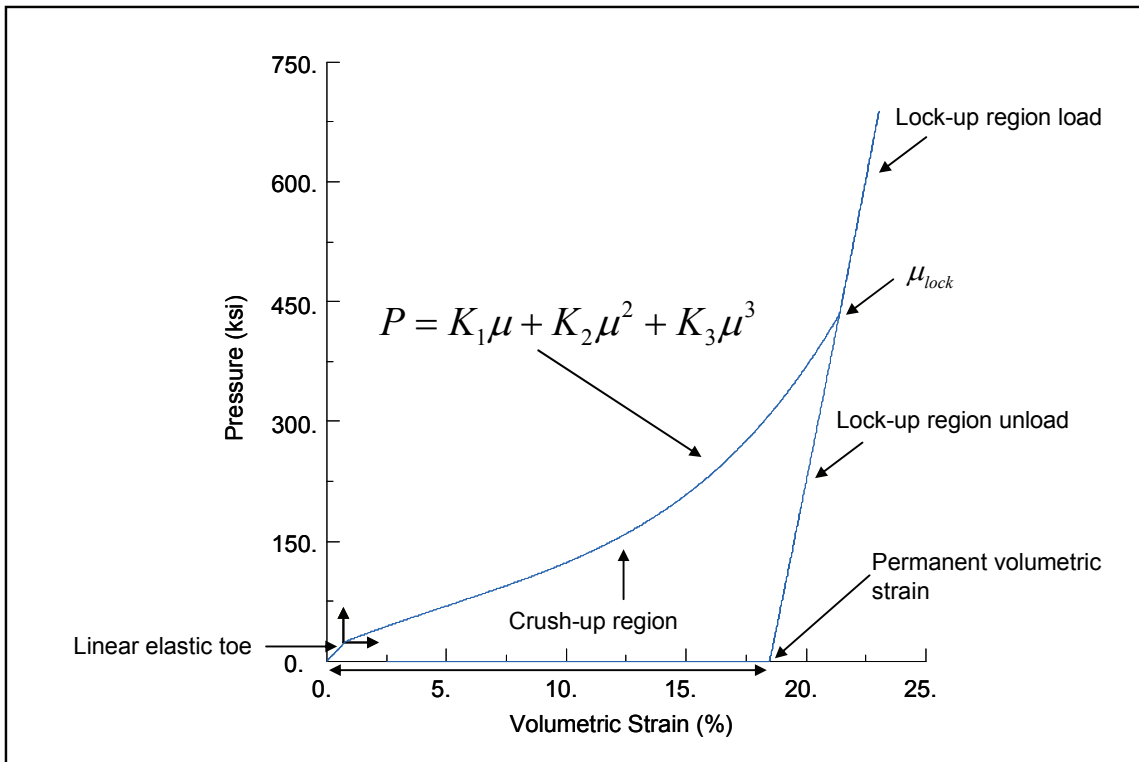


Figure 1. The AFC pressure-volume model.

The crushing region is characterized by permanent volume compaction and follows the following third-order polynomial equation.

$$P = K_1\mu + K_2\mu^2 + K_3\mu^3 \quad (1)$$

where  $K_1$ ,  $K_2$ , and  $K_3$  are input parameters,  $P$  is the mean normal stress (pressure), and  $\mu$  is a measure of volumetric strain that is equal to the ratio of the initial volume minus the current volume to the current volume, i.e.,  $(V_0-V)/V$ . It should be noted that this equation uses the soil mechanics sign convention (compression > 0), which means that the pressure ( $P$ ), as computed by the previous equation, is equal to the first invariant of the stress tensor ( $I_1$ ) multiplied by -1, i.e.,  $I_1 = -P$ . In the crushing region, unloading and reloading are nonlinear with the bulk modulus varying linearly between  $K_e$  and  $K_{lock}$  as  $\mu$  varies between  $U_{crush}$  and  $U_{lock}$ . However, since the change in  $\mu$  during a typical unload-reload cycle in the crush zone is generally only a small percentage of the value of  $(U_{lock} - U_{crush})$ , the response in most cases is nearly linear.

The linear elastic locking region in the model is defined by a locking bulk modulus ( $K_{lock}$ ) and occurs for volume strains above the locking value for

volumetric strain ( $U_{lock}$ ). Unloading and reloading in the locking region are purely linear elastic and also follow the locking bulk modulus ( $K_{lock}$ ).

The tensile hydrostatic behavior of the model is always defined by linear elastic behavior and follows a bulk modulus that is between the elastic bulk modulus ( $K_e$ ) and the locking bulk modulus ( $K_{lock}$ ), depending on the level of permanent volumetric crushing.

Next, we will describe the shear behavior of the model, which includes material yielding, plastic flow, and damage. Notice that an engineering mechanics sign convention has been used; hence, the mean normal stress (pressure) values less than zero denote compression. The compression yield surface is represented by the following two equations, depending on whether the hydrostatic component of the stress state is in compression or tension.

For stress states where the first invariant of the stress tensor ( $I_1$ ) is less than or equal to zero (indicative of compression), the failure surface is expressed as

$$S_Y = (C_1 - (C_2 + (C_1 - C_2)D)e^{A_n I_1} - C_4 I_1)/(1 + C_3 \ln(\dot{\varepsilon}_n)) \quad (2)$$

where  $C_1$ ,  $C_2$ ,  $C_3$ ,  $C_4$ , and  $A_n$  are constants that are greater than or equal to zero,  $D$  is a damage parameter that varies between 0 and 1, and  $\dot{\varepsilon}_n$  is an effective deviatoric strain rate that is normalized to a reference rate that is provided as input. It should also be noted that the values of  $C_1$  and  $C_2$  must satisfy the constraint  $C_1 \geq C_2$ .

For stress states where the first invariant of the stress tensor ( $I_1$ ) is greater than zero (indicative of tension), the failure surface is expressed as

$$S_Y = (C_1 - (C_2 + (C_1 - C_2)D))(1 + C_3 \ln(\dot{\varepsilon}_n))(T_{max} - I_1)/T_{max} \quad (3)$$

where  $T_{max}$  is the maximum allowable tensile pressure and the value of  $S_y$  is restricted to values that are greater than or equal to zero.

The third-invariant dependence of the failure surface is computed using the Lode angle (Chen and Han 1988). For example, a discrete extension failure surface value is computed by first computing the value of the compression failure surface at the stress state of interest and then

multiplying the compression failure surface value by a factor that is a function of the third invariant of the deviatoric stress tensor. Specifically, the Lode angle is computed, and then the value of the aforementioned factor is computed by evaluating either the William-Warnke Lode function or the Gudehus Lode function (Fossum and Brannon 2006). A typical failure surface is shown in Figure 2.

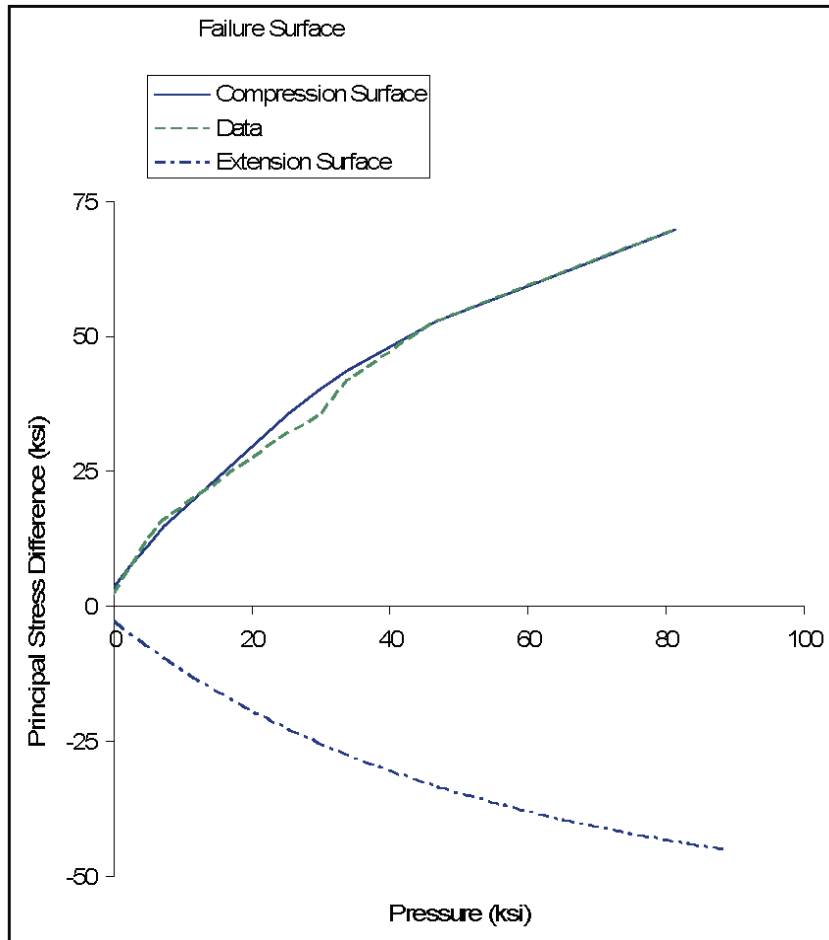


Figure 2. AFC failure surface fit to WES5000 concrete data.

As stated previously, our constitutive model also accounts for material damage that develops during the course of stress/strain loading histories. This material damage effectively provides a reduced failure surface due to excessive plastic shear strain as well as excessive hydrostatic crushing. The value of material damage is quantified using a scalar damage parameter ( $D$ ) that is computed by evaluating the following damage equation.

$$D = \sum \left( \frac{\Delta \varepsilon_p}{-I_1 D_1} + \frac{\Delta \mu_p}{1.5 U_{lock}} \right) \quad (4)$$

where  $D_1$  is an input parameter that is greater than zero, values of the expression  $(-I_1 D_1)$  are restricted to values greater than 0.01,  $\Delta\varepsilon_p$  is an increment in the effective deviatoric plastic strain,  $\Delta\mu_p$  is an increment of volumetric plastic strain, and  $U_{lock}$  is the locking volumetric strain value previously described. Notice that the material damage parameter ( $D$ ) is included in calculation of the failure surface as shown above in Equations 2 and 3. Since damage values that are greater than or equal to one are assumed to correspond to fully damaged material, and Equations 2 and 3 require damage values that are less than or equal to one; computed values of  $D$  that are greater than 1 are simply reset to a value of 1.0 in the code.

## Model fitting algorithm

The problem of determining parameters for a constitutive model can be cast in the form of a constrained optimization problem. Specifically, the fitting algorithms are used to minimize the weighted sum of squared residuals merit function given by

$$\Phi(\bar{a}) = \sum_{i=1}^n w_i [\sigma_i - \hat{\sigma}_i(\varepsilon, \bar{a})]^2 \quad (5)$$

where  $\sigma_i$  represents the stress values measured in material property experiments,  $\hat{\sigma}_i$  represents the stress values predicted by the material model that are a function of the strain ( $\varepsilon$ ) and the vector of material model parameter values ( $\bar{a}$ ),  $w_i$  is a weighting factor, and the parameter values are subject to a set of constraints, e.g.,  $\bar{a}_{\min} \leq \bar{a} \leq \bar{a}_{\max}$ .

The only independent variables in Equation 5 are the set of unknown material model parameters  $\bar{a}$ . Therefore, the model fitting problem consists of selecting a set of material model parameters that minimizes the error, in a least squares sense, between the predicted stress values and the stress values measured experimentally.

The merit function represented by Equation 5 can become extremely complex and highly nonlinear due to the complexity/nonlinearity of both the constitutive models and the material behaviors observed in laboratory experiments. Although direct search methods often converge quickly for well-behaved merit functions, the complexity of the merit function makes it very difficult for conventional gradient-based direct search methods to

converge to an optimum solution that minimizes the aforementioned merit function. For that reason, the VPL code employs Continuous Evolutionary Algorithms (CEA; Furukawa et al. 2002) that are used in conjunction with the gradient-based Levenberg-Marquardt Algorithm (LMA; Marquardt 1963). The CEA methods provide the ability to find optimum solutions for extremely complex merit functions, while the LMA approach reduces the computation time by quickly moving the candidate solutions toward the regions of the parameter space that are more likely to contain the optimum solution.

In CEA, a trial solution is a vector representation of the parameter set ( $\bar{\alpha}$ ). The algorithm employed in this work selects a number ( $m$ ) of initial trial solutions where the parameter values in each of the  $m$  vectors are selected at random. The following operations are then completed in a loop that is terminated only when a convergence criterion is satisfied, i.e., the merit function has reached an acceptably small value.

The operations performed each time through the loop (in each iteration), in the order of calculation, are: (1) evaluate the merit function ( $\Phi$ ) for each of the  $m$  trial solutions (individuals), (2) identify and save the solution that provided the smallest value of the merit function for use in the next iteration (the most fit individual), (3) use the method of steepest descent, starting at the best solution (the elite individual identified in the previous operation) to determine a new trial solution that will replace the worst solution (least fit individual), and (4) recombine the current trial solutions to obtain the additional ( $m-1$ ) trial solutions required, where the probability of a vector's participation in the recombination (mating) process depends on its merit function value (fitness). It is clearly seen by the vocabulary used in the description of CEA algorithms that they are inspired by biological evolution processes.

The recombination (mating) algorithm used in the current work is represented by the following equations.

$$\begin{aligned}\bar{\alpha}_i^* &= (1 - \alpha)\bar{\alpha}_i + \alpha\bar{\alpha}_j \\ \bar{\alpha}_j^* &= \alpha\bar{\alpha}_i + (1 - \alpha)\bar{\alpha}_j\end{aligned}\quad (6)$$

where  $\alpha$  is a scalar value that is defined by a normal distribution with a mean of 0 and a specified standard deviation, and the parents ( $\bar{\alpha}_i$  and  $\bar{\alpha}_j$ )

are selected at random from the mating pool. Since the probability of a solution (individual) being selected to participate in the mating process depends on the value of its merit function (level of fitness), this search algorithm moves toward a solution that minimizes the merit function and provides a best fit to the material property data used in the merit function.

## Model fits

We fit our constitutive material model using the available laboratory material property data for two different conventional strength concrete materials, which we shall call materials WES5000 and CSPC. These fits were generated using the automatic fitting program described above in conjunction with a finite element driver program that can simulate the appropriate loading and strain conditions (i.e., boundary conditions) from results of the laboratory material property testing. Specifically, we used quasi-static hydrostatic compression, unconfined compression, uniaxial strain compression, triaxial compression, and direct-pull laboratory material property data to generate our material model constants. It should be noted that we did not have any rate-dependent data and thus could not fit the failure surface rate parameter using the automatic fitting code. Instead, this parameter was fit using numerical simulations in conjunction with the projectile penetration experiments described below.

The automatically generated fit to concrete material WES5000 is shown in Figures 2 through 4. These figures employ the soil mechanics sign convention where compression is positive. As shown in Figure 2, the model is able to differentiate between the extension and compression failure surfaces due to the inclusion of the third invariant. The compression failure surface data were used by the automatic fitting code to determine the material model parameters that define the shape of the failure surface. Since no extension data were available, the location of the extension failure surface had to be assumed. The parameters that define the pressure-volume behavior of the model were determined by automatically fitting the uniaxial strain data shown in Figure 3. The curvature of the material model curve in Figure 3 is a result of the form of the pressure-volume equation in conjunction with the additional requirement that the predicted curve must extrapolate to high pressures in a reasonable fashion. The fitting code determined the damage parameter by matching the softening behavior observed in various triaxial compression tests, e.g., Figure 4.

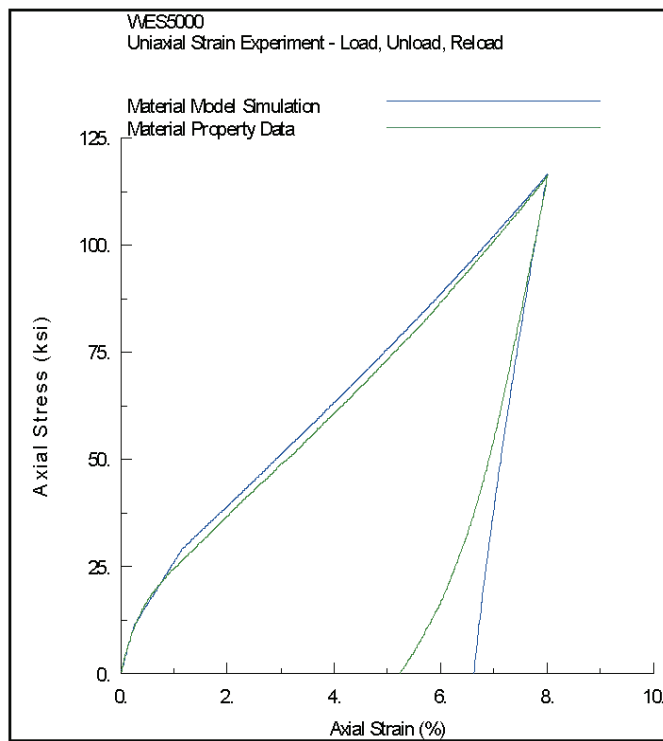


Figure 3. AFC model fit to WES5000 uniaxial strain test data.

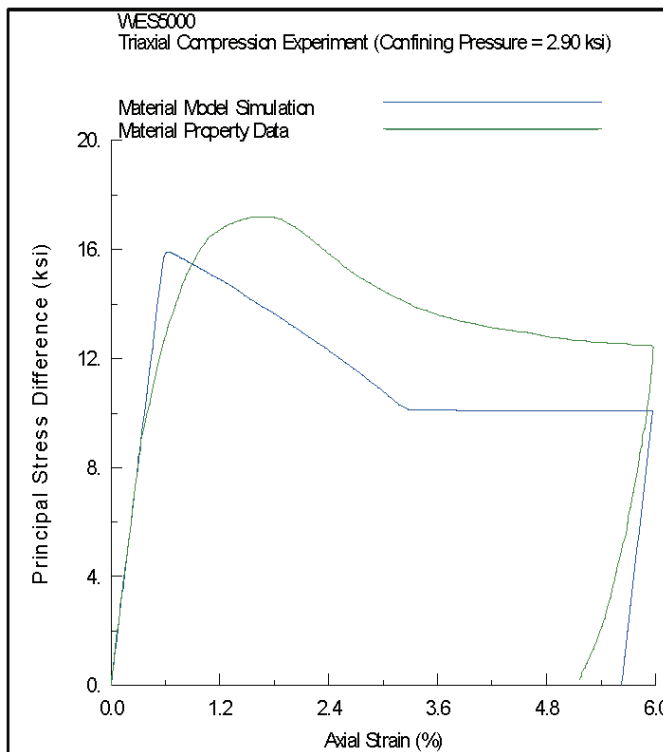


Figure 4. AFC model fit to WES5000 triaxial compression data.

The automatically generated fit to concrete material CSPC is shown in Figures 5–7. These figures also employ the soil mechanics sign convention where compression is positive. As shown in Figure 5, the model is again able to differentiate between the extension and compression failure surfaces due to the inclusion of the third invariant. The compression failure surface data were used by the automatic fitting code to determine the material model parameters that define the shape of the failure surface.

Since no extension data were available, the location of the extension failure surface had to be assumed. The parameters that define the pressure-volume behavior of the model were determined by automatically fitting the uniaxial strain data shown in Figure 6. Finally, the fitting code determined the damage parameter by matching the softening behavior observed in various triaxial compression tests, e.g., Figure 7.

The automatic fitting code can be used in a number of different ways to obtain model fits. One strategy is to fit all of the parameters at the same time to the full set of available data. This strategy requires the most computational time because the size of the vector storing the parameter values ( $\bar{a}$ ) is large (~15), i.e., the search space is very large. Another

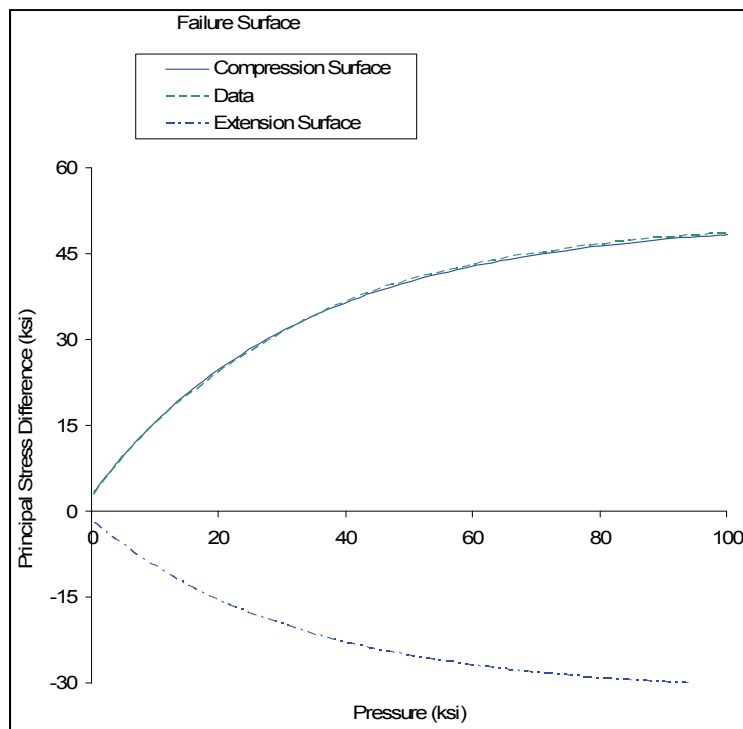


Figure 5. AFC failure surface fit to CSPC concrete data.

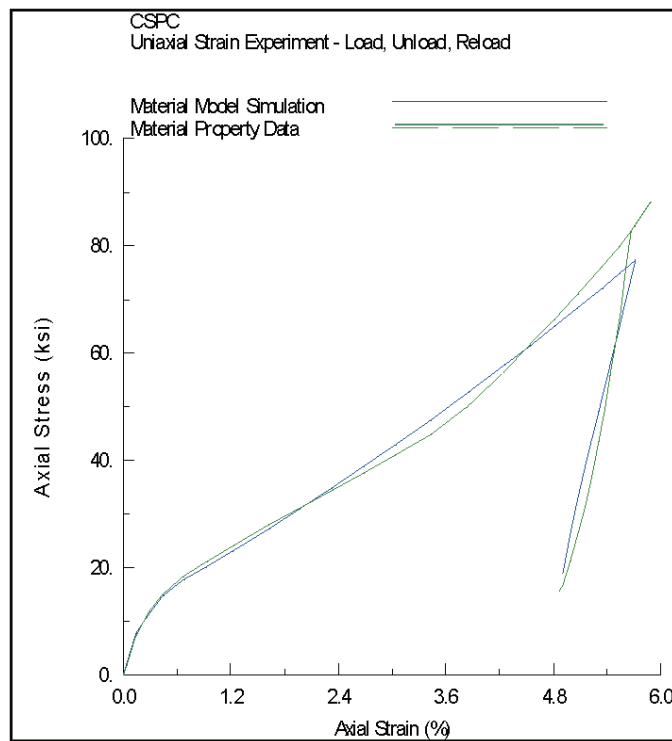


Figure 6. AFC model fit to CSPC uniaxial strain test data.

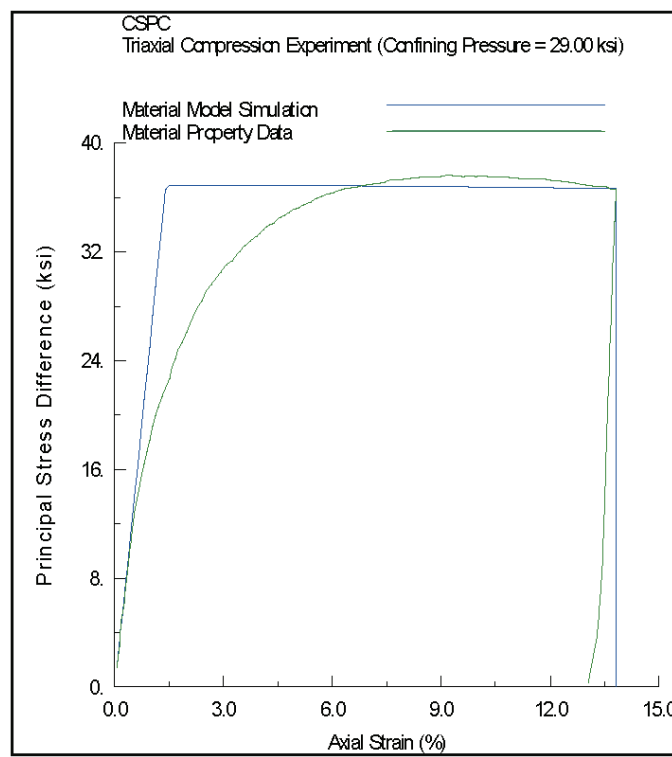


Figure 7. AFC model fit to CSPC triaxial compression data.

strategy is to first fit the failure surface parameters to failure surface data and then fit the pressure-volume parameters to data separately. This approach reduces the computational time and gives the analyst more control over the process. A variation of the latter strategy was used to develop the model fits presented herein. Specifically, the failure surface was first fit to the available compression failure surface data. That simulation provides values for parameters C<sub>1</sub>, C<sub>2</sub>, C<sub>4</sub>, and A<sub>n</sub>. That is, the dimension of the parameter vector ( $\bar{a}$ ) was 4. The pressure-volume variables and the shear modulus were then fit to uniaxial strain data that provided values for eight parameters, i.e., the size of the parameter vector ( $\bar{a}$ ) was 8. Finally, the damage parameter (D<sub>1</sub>) was fit to triaxial compression data. The number of trial solutions (m) typically used varies from 11 to 21. The fits presented herein were generated using m = 21. The number of iterations required for convergence typically varies between 50 and 500 depending on the quality of the initial trial solution and the size of the search space. The entire fitting process usually requires very little computer time, even when it is conducted on a laptop computer. An example simulation, using 21 trial solutions (m = 21) to fit eight parameters to uniaxial strain data, completed 100 iterations in 26 sec of CPU time on a 3-GHz laptop computer.

## **Model implementation and testing**

We implemented the constitutive material model described above into the EPIC hydrocode (Johnson et al. 2001). The implementation was relatively straightforward, and we will not discuss this in any more detail. In order to test the response of this material model, we performed numerical simulations of various penetration experiments conducted at ERDC. These simulations included both projectile perforation as well as deep penetration. We discuss the results from these simulations along with corresponding comparisons to the experimental data in the next two chapters.

### 3 Projectile Perforation Simulations

#### Perforation experiments

We based our calculations on a series of perforation experiments conducted at ERDC (Cargile 1999). The experiments were conducted with a 2.3-kg ogival nose projectile ( $CRH = 3.0$ ,  $L/D = 7.0$ , and  $D = 50.8$  mm) launched into three unreinforced concrete slabs with thicknesses of 127, 216, and 254 mm. Each of the slabs was constructed in a steel culvert form with a nominal diameter of 1.52m, providing a near infinite width for these perforation events, i.e., a target width to projectile diameter ratio of 30. All the experiments were conducted under “near” normal impact conditions, i.e., angle-of-obliquity and angle-of-attack were less than 1 deg, with an impact velocity of approximately 310 m/sec. The slabs were constructed with WES5000 concrete. The experiments were designed to challenge the numerical simulations by providing three distinctly different target responses, i.e., a relatively thin slab providing little resistance, a typical slab providing nominal resistance, and finally a relatively thick slab approaching the perforation limit thickness of the projectile. Thereby, these experiments provide a good baseline for comparison with the impact and exit phase of projectile penetration (Cargile 1999), which is typically characterized by low confinement stress states under compression, extension, and/or tension of the target material. All the experiments resulted in complete perforation of the concrete slabs. Figure 8 shows representative results from these perforation experiments. Shown are typical projectile exit velocities and the posttest concrete damage in terms of the final impact and exit crater profiles.

#### 2D perforation simulations

We conducted 2D axisymmetric EPIC simulations of the perforation experiments discussed above and illustrated in Figure 8. Our finite element models were developed to focus on the target responses. Therefore, we used a relatively low fidelity input for the projectile (617 elements) and a high fidelity input for each of the target slabs, i.e., 4919, 8379, and 10001 elements for the 127-, 216-, and 254-mm slabs, respectively. It should be noted that our finite element models use linear triangular elements. We used the experimentally determined projectile exit velocities and the final crater profiles from Figure 8 as the metrics to evaluate our simulations.

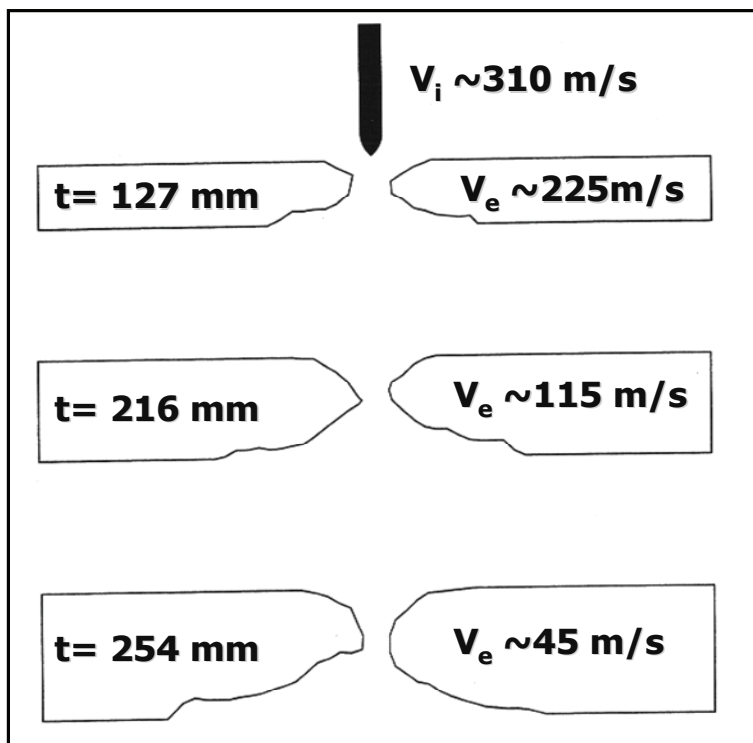


Figure 8. Representative results from prior perforation experiments; impact ( $V_i$ ) and exit ( $V_e$ ) velocities and final crater shapes are shown.

Figure 9 shows a snapshot at 10 msec from the 127-mm-slab EPIC simulations. The crater shape observed in the relevant experiment is superimposed on the target shown in Figure 9. The predicted exit velocity is in very close agreement to the value recorded in the experiment (see Figure 8), and the crater shape is reasonable.

Figure 10 shows a snapshot at 10 msec from the 216-mm-slab EPIC simulations. The crater shape observed in the relevant experiment is again superimposed on the target shown in Figure 10. The predicted exit velocity is in good agreement with the value recorded in the experiment (see Figure 8), and the crater shape is also in close agreement with the experimental data.

Figure 11 shows a snapshot at 15 msec from the 254-mm-slab EPIC simulations. The crater shape observed in the relevant experiment is superimposed on the target. Since the target used in this example is close to the perforation limit thickness, this is a very challenging problem. However, in spite of that fact, the predicted exit velocity is reasonable, and the impact crater shape is in excellent agreement with the data. The predicted shape of the exit crater is reasonable but is smaller than the exit crater observed in the experiment.

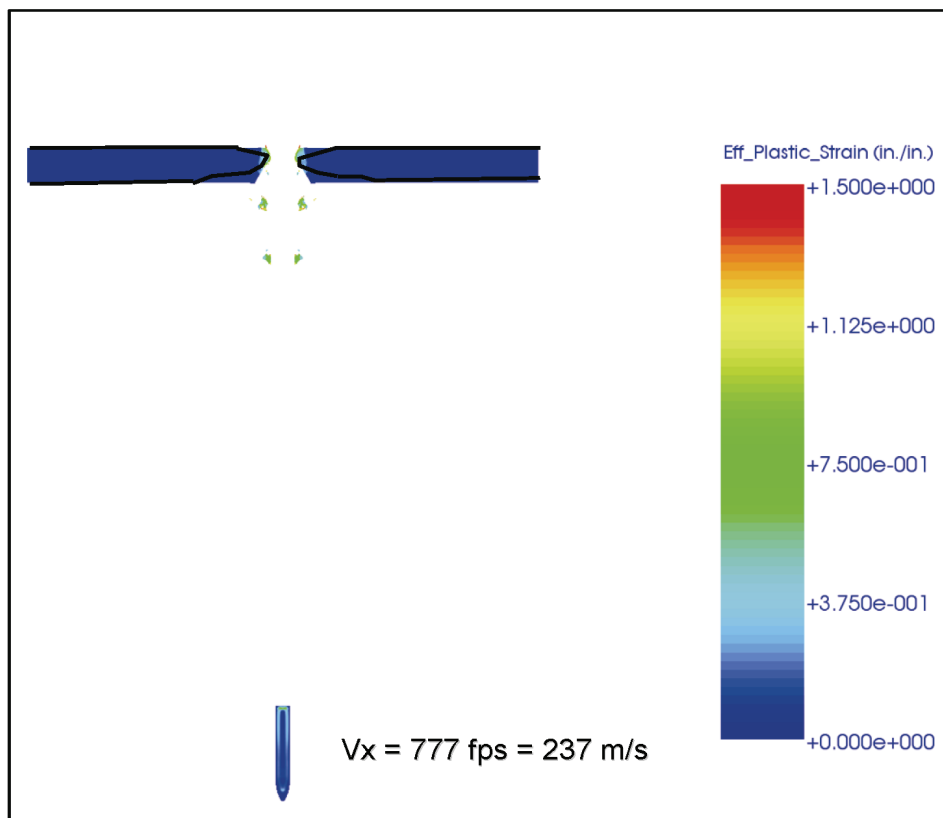


Figure 9. EPIC penetration simulation using the AFC model:  
127-mm-thick concrete target (time = 10 msec).

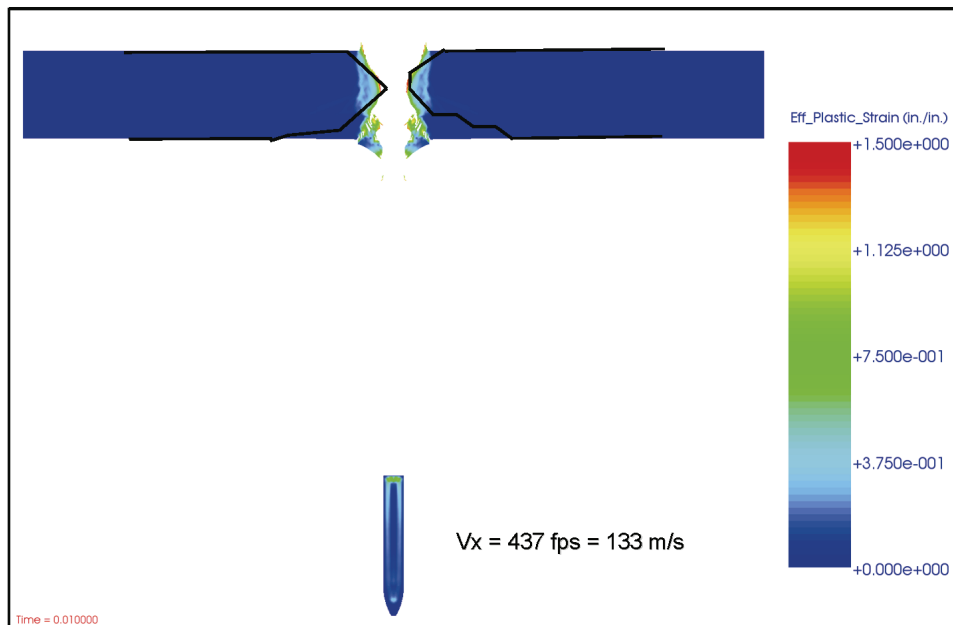
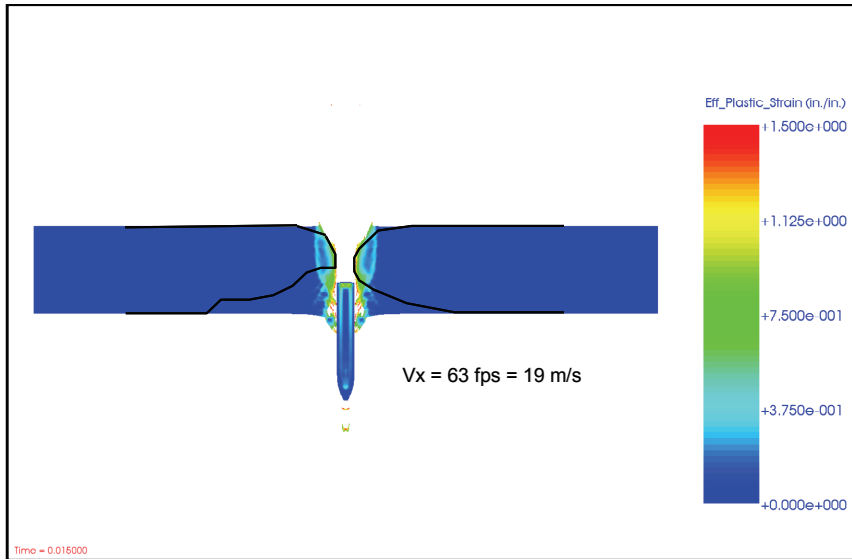


Figure 10. EPIC penetration simulation using the AFC model:  
216-mm-thick concrete target (time = 10 msec).



**Figure 11. EPIC penetration simulation using the AFC model:  
254-mm-thick concrete target (time = 15 msec).**

It is worth noting that the perforation problems presented in this section involve stress paths that exhibit a significant amount of extension stresses, e.g., as the projectile approaches the rear-face of the target. Consideration of the third invariant, and the reduction in the strength of the extension failure surface versus the compression failure surface, is an important factor for accurately predicting the exit velocity of the projectile (Frank and Adley 2007). Two-invariant models, such as the HJC model (Holmquist et al. 1993), tend to underpredict the exit velocity because the extension failure surface is assumed to be identical to the compression failure surface. This deficiency is sometimes compensated for by adjusting the model parameters to improve perforation predictions, but this is done at the expense of the quality of the model fit to the material property data. Since the AFC model is a three-invariant model, it is able to provide high-fidelity predictions of the perforation velocity while still using a model fit that properly fits the material property data.

## 4 Projectile Penetration Simulations

### Penetration experiments

We based these calculations on a series of penetration experiments also conducted at ERDC (Cargile 1999). The experiments were conducted with a 0.9-kg ogival nose projectile ( $CRH = 2.0$ ,  $L/D = 9.0$ , and  $D = 26.9$  mm) launched into a 1.22-m-diam by 1.83-m-thick target. These targets were designed to be almost a half-space providing a relatively large thickness and width, i.e., the target width to projectile diameter ratio was 45, and the target thickness to projectile diameter ratio was 68. The targets were unreinforced and constructed in a steel culvert form with the CSPC concrete material. All the experiments were conducted under “near” normal impact conditions, i.e., angle-of-obliquity and angle-of-attack were less than 1 deg. The impact velocities were varied from 277 to 800 m/sec. The experiments were designed to allow for near rigid-body penetration events, i.e., a robust thick-walled projectile. The data recorded from these experiments were depth of penetration versus impact velocity. None of the experiments resulted in the projectile penetrating more than half the target thickness. Thereby, these experiments provide a good baseline for comparison with the tunneling phase of projectile penetration (Cargile 1999), which is typically characterized by high confinement stress states under compression in the target material.

### 2D penetration simulations

We conducted 2D axisymmetric EPIC simulations of the penetration experiments discussed above. Our finite element models were developed to focus on the target responses, and therefore, we used a relatively low fidelity for the projectile (264 elements) and a higher fidelity for the target slab (14,960 elements). It should be noted that our finite element models used linear triangular elements. We used the experimentally determined projectile penetration depth as the metric to evaluate our simulations.

Figure 12a shows a snapshot at 1.2 msec from the 300-m/sec EPIC simulation, and Figure 12b shows a snapshot at 2 msec from the 800-m/sec EPIC simulation. As shown in Figure 12, these are deep penetration simulations where the projectile spends the majority of the event in a tunneling mode.

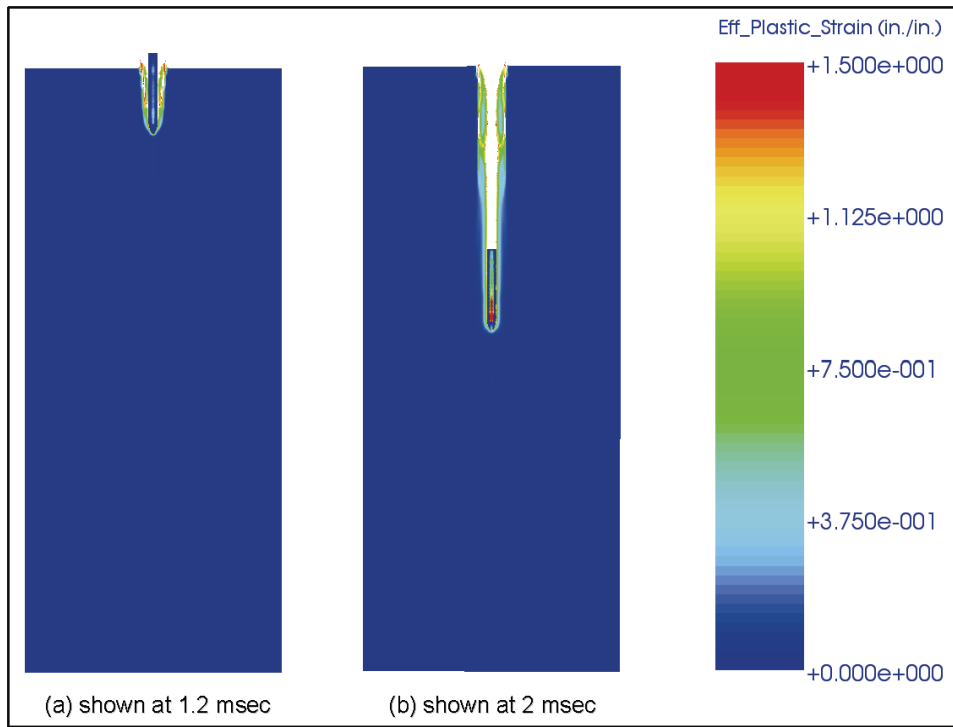


Figure 12. EPIC penetration simulations using the AFC model for impact velocities of (a) 300 m/s and (b) 800 m/s.

Figure 13 is a comparison of the penetration depth versus impact velocity for the EPIC simulations and the experimental data. The depth of penetration predictions are in close agreement with the experiments for the two lower velocity simulations. However, when the impact velocity approaches 800 m/sec, the fidelity of the predictions appears to decrease. The cause of the reduction in fidelity with increasing velocity is currently not known and is a current topic of the author's research.

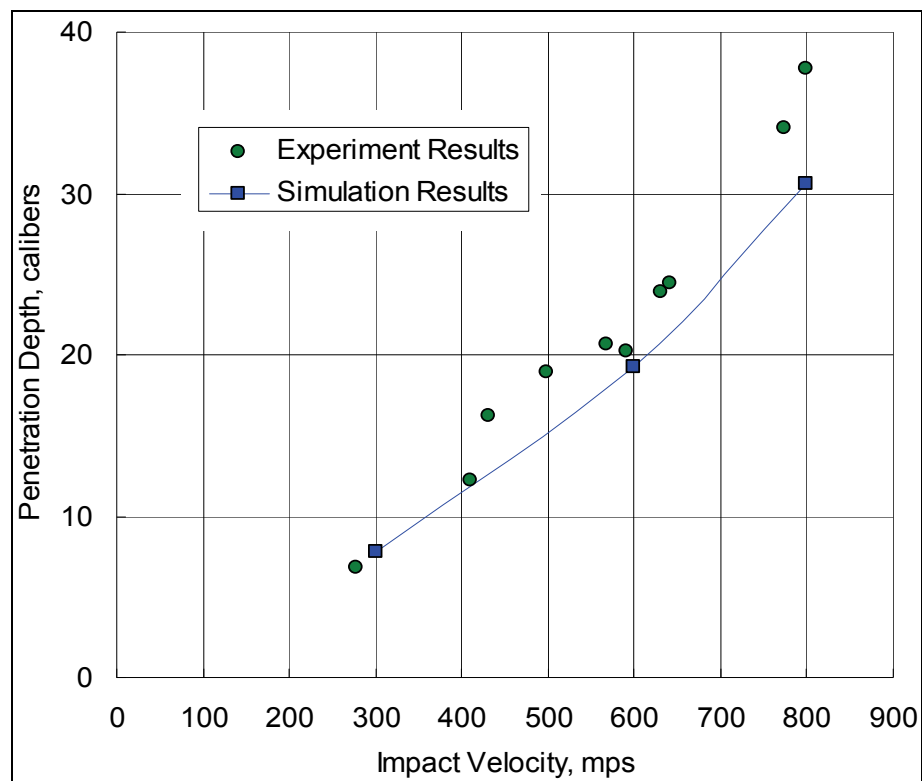


Figure 13. EPIC penetration simulation results using the AFC model versus experimental data from ballistic experiments (Cargile et al. 1999).

## 5 Penetration Resistance Equation for CSPC

The VPL software package includes a one-dimensional finite element code that is used to solve cavity expansion simulations and a rigid-body trajectory code that uses penetration resistance (PR) equations to model the target material. The process used to develop PR equations is briefly discussed below. A more comprehensive discussion of this topic is available in the paper by Adley et al. (2007).

The methodology employed in VPL to develop PR equations involves using the finite element method to solve the equations governing the dynamic expansion of a cavity in a target material. The first step in the process involves the solution of a series of cavity expansion problems where each problem is defined as the opening of a cavity at a constant expansion velocity. Each cavity expansion solution runs until the radial (normal to cavity wall) stress approaches a constant value. Each of those solutions represents a point in radial stress versus radial velocity space.

The second step in the process involves the determination of the quadratic equation that best fits the aforementioned data points in a least squares sense. This equation represents the resistance of the target to the opening of a cavity as a function of the cavity expansion velocity.

The third step requires the transformation of the cavity expansion resistance equation to a penetration resistance equation. This is accomplished by replacing the radial cavity expansion velocity with the component of the projectile's velocity that is normal to the surface of the projectile at the point under consideration, e.g., the center of an element face that is located in the outer surface of the finite element mesh of the projectile. The resisting stress predicted by the transformed equation is then interpreted as the normal stress that is acting on the surface of the projectile at the point under consideration, i.e., the penetration resistance of the target.

The completion of the aforementioned three tasks results in the development of the penetration resistance equation. The equation can then be implemented in a rigid-body trajectory code to study the loading history predicted by the penetration resistance equation and the fidelity of the

penetration trajectory predictions. Assuming the results of that validation process produce encouraging results, the equation can then be implemented in a finite element code to study the structural response of projectiles subjected to impact and penetration events.

The AFC concrete model and the fit for CSPC concrete discussed previously is used in conjunction with the cavity expansion code to develop PR equations for CSPC concrete. The PR equation developed by using spherical cavity expansion is shown in Figure 14 along with the numerical data points that represent the cavity expansion solutions. The PR equation developed by using cylindrical cavity expansion is shown in Figure 15 along with the numerical data points that represent the cavity expansion solutions. The PR equations shown in Figures 14 and 15 are used in the VPL trajectory code to simulate the deep penetration experiments discussed in the previous section, i.e., the PR equation is used to model the target. A comparison between the VPL predictions and the experimental data is shown in Figure 16. As shown in Figure 16, the fidelity of the PR predictions rivals the fidelity of the full finite element simulations presented in the previous section, even though the VPL simulations require only a small fraction of the computer time.

It is also worth noting that the PR equation, based on cylindrical cavity expansion, provides more accurate predictions than the PR equation based on the more commonly used spherical cavity expansion formulation. This is most likely due to the fact that the ogive nose of the projectile used in the experiments creates a stress field in the concrete target that is more consistent with cylindrical cavity expansion. This observation led the authors to develop PR equations that use combinations of the cylindrical and spherical PR equations that are based on the local shape of the nose of the projectile (Adley et al. 2007).

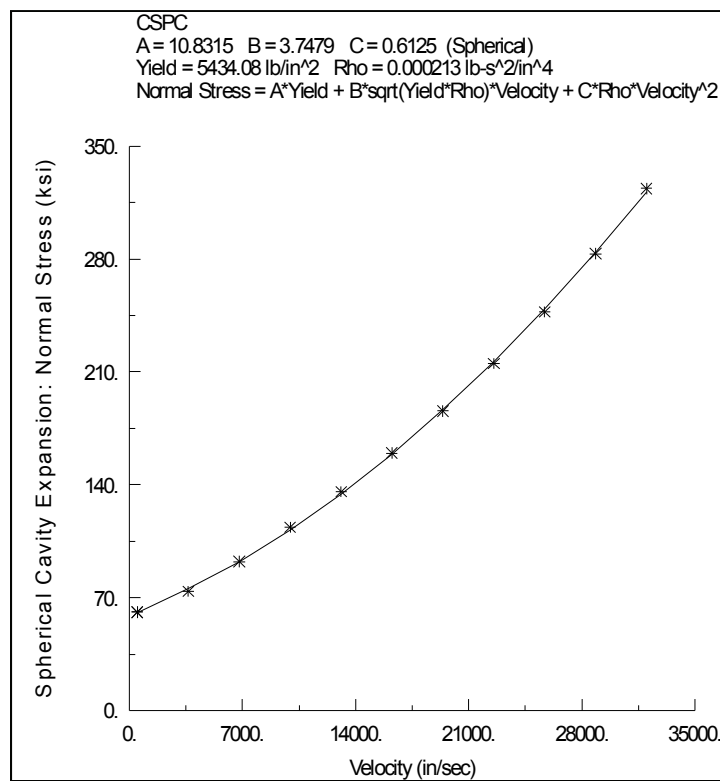


Figure 14. Spherical CSPC PR equation developed in the VPL code.

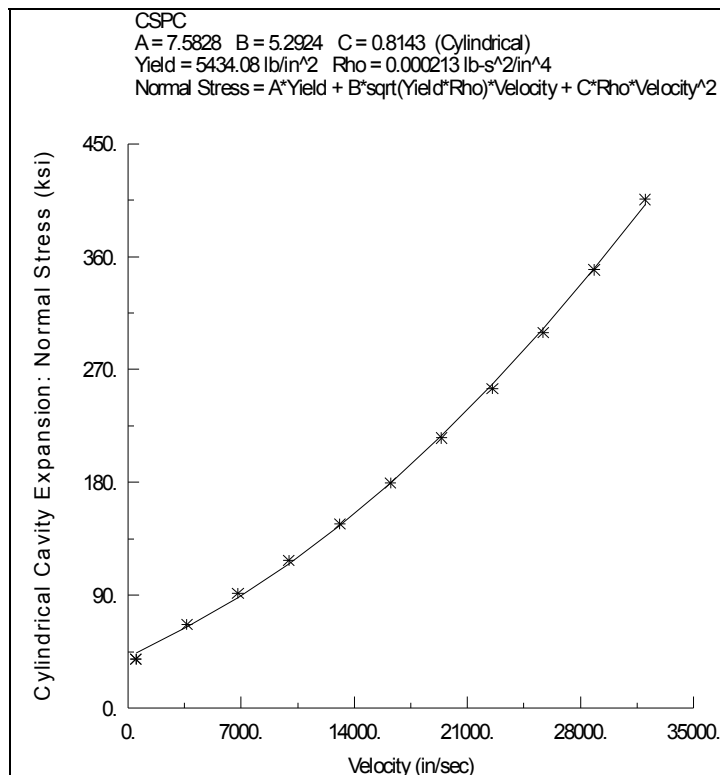


Figure 15. Cylindrical CSPC PR equation developed in the VPL code.

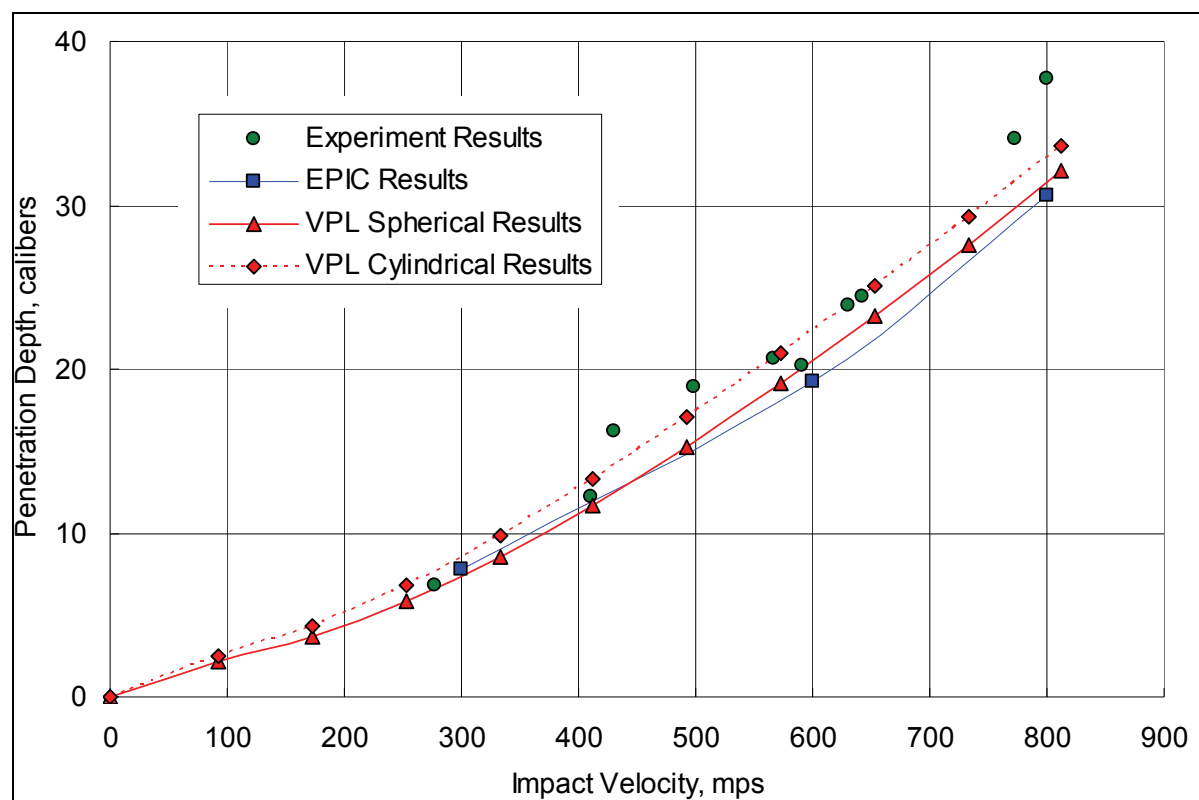


Figure 16. Comparison of EPIC and VPL predictions with experimental data.

## 6 Conclusions

A new three-invariant constitutive model for concrete called the AFC model was developed. The automatic fitting algorithms used to determine the model parameters were discussed and used to determine AFC model fits for two concrete materials. The AFC model was implemented in the EPIC finite element code and used to conduct numerical simulations of projectile perforation and penetration experiments in order to validate the new model.

Obtaining accurate predictions of exit velocities in perforation problems, where the stress paths exhibit a considerable amount of extension stresses, is a challenge for a material model. Two-invariant models, such as the HJC model (Holmquist et al. 1993), tend to underpredict the exit velocity because the extension failure surface in the model is assumed to be identical to the compression failure surface. This deficiency is sometimes compensated for by adjusting the model parameters to improve perforation predictions, but this is done at the expense of the quality of the model fit to the material property data. Since the AFC model is a three-invariant model, it was able to provide high-fidelity predictions of the perforation velocity, while still using a model fit that properly fits the material property data. The AFC model was also able to provide accurate predictions of penetration depth in deep penetration problems that involve high pressures and a high degree of confinement.

The validated AFC model was used in the VPL code to develop PR equations for the CSPC concrete. The PR equations were used in a rigid-body trajectory code to create a fast-running penetration model. The PR equation, based on a cylindrical cavity expansion formulation, performed significantly better than the PR equation based on the more commonly used spherical cavity expansion formulation, especially at the higher impact velocities.

The numerical simulations conducted using the AFC model provided predictions of penetration depths, perforation velocities, and crater shapes that compared well with experimental data. These initial results indicate that the AFC model shows significant promise for being a useful constitutive model

for use in simulations involving concrete and high-strength geologic materials.

The PR equations developed in the VPL code provided excellent predictions of penetration depth when compared to the results of the deep penetration experiments. This indicates that the VPL code should become a very useful tool for developing PR equations for new target materials of interest.

## References

- Adley, M. D., J. D. Cargile, S. A. Akers, and B. Rohani. 1996. Numerical simulation of projectile penetration into concrete. *Proceedings, 14th U.S. Army Symposium on Solid Mechanics, Myrtle Beach, SC.*
- Adley, M. D., A. O. Frank, K. T. Danielson, S. A. Akers, J. D. Cargile, B. C. Patterson, and S. Termaath. 2007. Generating penetration resistance functions with a Virtual Penetration Laboratory (VPL): applications to projectile penetration and structural response simulations. *Proceedings, 48th AIAA/ASME/ASCE/AHS/ASC Structures, Structural Dynamics, and Materials Conference, Waikiki, HI.*
- Akers, S. A., M. D. Adley, and J. D. Cargile. 1995. Comparison of constitutive models for geologic materials used in penetration and ground shock calculations. *Proceedings, 7th International Symposium on the Interaction of Conventional Munitions with Protective Structures, Mannheim, FRG.*
- Cargile, J. D. 1999. *Development of a constitutive model for numerical simulations of projectile penetration into brittle geomaterials.* Technical Report SL-99-11. Vicksburg, MS: U.S. Army Engineer Research and Development Center.
- Chen, W. F., and D. J. Han. 1988. *Plasticity for structural engineers.* New York, NY: Springer-Verlag.
- Fossum, A. F., and R. M. Brannon. 2006. On a viscoplastic model for rocks with mechanism-dependent characteristic times. *Acta Geotechnica* 1:89–106.
- Frank, A. O., and M. D. Adley. 2007. On the importance of a three-invariant model for simulating the perforation of concrete slabs. *Proceedings, 78th Shock and Vibration Symposium, Philadelphia, PA.*
- Frew, D. J., J. D. Cargile, and J. Q. Ehrgott. 1993. WES geodynamics and projectile penetration research facilities. *Proceedings, Symposium on Advances in Numerical Simulation Techniques for Penetration and Perforation of Solids, ASME Winter Annual Meeting, New Orleans, LA.*
- Furukawa, T., T. Sugata, S. Yoshimura, and M. Hoffman. 2002. An automated system for simulation and parameter identification of inelastic constitutive models. *Computer Methods in Applied Mechanics and Engineering* 191:2235–2260.
- Holmquist, T. J., G. R. Johnson, and W. H. Cook. 1993. A computational constitutive model for concrete subjected to large strains, high strain rates, and high pressures. *Proceedings, Fourteenth International Symposium on Ballistics, Quebec City, Canada.*
- Johnson, G. R., R. A. Stryk, and S. R. Beissel. 2001. *User instructions for the 2001 version of the EPIC code.* Hopkins, MN: Alliant Techsystems, Inc.
- Marquardt, D. 1963. An algorithm for least-squares estimation of nonlinear parameters. *SIAM Journal on Applied Mathematics* 11:431–441.



## **REPORT DOCUMENTATION PAGE**

Form Approved  
OMB No. 0704-0188

Public reporting burden for this collection of information is estimated to average 1 hour per response, including the time for reviewing instructions, searching existing data sources, gathering and maintaining the data needed, and completing and reviewing this collection of information. Send comments regarding this burden estimate or any other aspect of this collection of information, including suggestions for reducing this burden to Department of Defense, Washington Headquarters Services, Directorate for Information Operations and Reports (0704-0188), 1215 Jefferson Davis Highway, Suite 1204, Arlington, VA 22202-4302. Respondents should be aware that notwithstanding any other provision of law, no person shall be subject to any penalty for failing to comply with a collection of information if it does not display a currently valid OMB control number. **PLEASE DO NOT RETURN YOUR FORM TO THE ABOVE ADDRESS.**

<b>1. REPORT DATE (DD-MM-YYYY)</b> November 2010	<b>2. REPORT TYPE</b> Final report	<b>3. DATES COVERED (From - To)</b>		
<b>4. TITLE AND SUBTITLE</b>  The Advanced Fundamental Concrete (AFC) Model			<b>5a. CONTRACT NUMBER</b>	
			<b>5b. GRANT NUMBER</b>	
			<b>5c. PROGRAM ELEMENT NUMBER</b>	
<b>6. AUTHOR(S)</b>  Mark D. Adley, Andreas O. Frank, Kent T. Danielson, Stephen A. Akers, and James L. O'Daniel			<b>5d. PROJECT NUMBER</b>	
			<b>5e. TASK NUMBER</b>	
			<b>5f. WORK UNIT NUMBER</b>	
<b>7. PERFORMING ORGANIZATION NAME(S) AND ADDRESS(ES)</b>  U.S. Army Engineer Research and Development Center Geotechnical and Structures Laboratory 3909 Halls Ferry Road Vicksburg, MS 39180-6199			<b>8. PERFORMING ORGANIZATION REPORT NUMBER</b>	
			ERDC/GSL TR-10-51	
<b>9. SPONSORING / MONITORING AGENCY NAME(S) AND ADDRESS(ES)</b>  Headquarters, U.S. Army Corps of Engineers Washington, DC 20314-1000			<b>10. SPONSOR/MONITOR'S ACRONYM(S)</b>	
			<b>11. SPONSOR/MONITOR'S REPORT NUMBER(S)</b>	
<b>12. DISTRIBUTION / AVAILABILITY STATEMENT</b> Approved for public release; distribution is unlimited.				
<b>13. SUPPLEMENTARY NOTES</b>				
<b>14. ABSTRACT</b> A new constitutive model, the Advanced Fundamental Concrete (AFC) model, was developed for simulating the penetration of projectiles into concrete. Although relatively simple, the model is very robust and fast-running and contains a three-invariant failure surface and nonlinear loading and unloading in hydrostatic compression. This new capability is an adjunct to the Virtual Penetration Laboratory (VPL) software package to address the challenges of determining penetration resistance (PR) equations for high-strength concretes. The Continuous Evolutionary Algorithms automatic fitting routine was used to fit the new model to laboratory mechanical properties for two high-strength concretes. These model fits were implemented into a finite-element code and used in numerical simulations of projectile perforation and penetration experiments. Initial comparisons between results of the simulations and the experiments indicate that the AFC model shows significant promise for use in numerical simulations involving concrete and high-strength geologic materials. Finally, the AFC model in conjunction with the VPL software package was used to develop a PR equation for a high-strength concrete.				
<b>15. SUBJECT TERMS</b> Advanced Fundamental Concrete (AFC) model      Concrete Modeling      Projectile penetration Simulation				
<b>16. SECURITY CLASSIFICATION OF:</b>			<b>17. LIMITATION OF ABSTRACT</b>	<b>18. NUMBER OF PAGES</b>
a. REPORT UNCLASSIFIED	b. ABSTRACT UNCLASSIFIED	c. THIS PAGE UNCLASSIFIED		34
			<b>19b. TELEPHONE NUMBER (include area code)</b>	

